SUPPLEMENTAL MATERIALS AND METHODS

Atlas Generation Dataset

T1-weighted 3D-MPRAGE MR images were acquired after administration of MR contrast agent (Magnevist) with the following parameters: TE = 1.64 ms, TR = 2,530 ms, TI = 1,200 ms, reconstruction matrix size = 256 × 256 × 256 voxels with voxel size = 1 × 1 × 1 mm, 4 averages, total acquisition time = 5 min 53 s.

CT images (LightSpeed QX/I; GE Healthcare) were acquired following the clinical protocol at MGH: 512 × 512 in-plane voxels, with voxel sizes ranging from 0.49 × 0.49 × 2.5 mm to 0.67 × 0.67 × 2.5 mm.

Atlas Validation Dataset

MR images were acquired simultaneously with the PET data using an MPRAGE sequence. The sequence parameters were as follows: for Copenhagen dataset (n = 7) TE = 2.44 ms, TR = 1,900 ms, TI = 900 ms, reconstruction matrix size = 512 × 512 × 192 voxels, voxel size = 0.49 × 0.49 × 1 mm, 1 average, total acquisition time = 05:02 min:s; and for Munich dataset (n = 9): TE = 2.44 ms, TR = 1,900 ms, TI = 900 ms, reconstruction matrix size = 256 × 240 × 160 voxels, voxel size = 1 × 1 × 1 mm, 1 average, total acquisition time = 05:01 min:s. A dual-echo Dixon-VIBE sequence was also acquired at both sites (TE = 1.23/2.46 ms, TR = 3.6 ms, flip angle = 10 degrees, reconstruction matrix = 192 × 126 × 128 voxels, 2.6 × 2.6 × 2.23 mm, total acquisition time = 19 s).

Low-dose CT images were acquired at both sites without contrast for all subjects on the same day as their PET/MR session using a Biograph 64 scanner (Siemens) with the following image parameters: 512 × 512 matrix size with 1.37 × 1.37 × 5 mm (n = 9) and 0.59 × 0.59 × 3 mm (n = 7) voxel sizes.

Atlas Generation Steps

MR Image Segmentation into 6 Tissue Classes (SPM8 New Segment). The SPM8 New Segment option allows MR images of the head to be segmented into gray matter (GM), white matter (WM), cerebrospinal fluid (CSF), soft tissue, bone, and air (*1*). Briefly, the method uses a probabilistic model that combines nonrigid image registration, bias correction, and tissue classification based on a mixture-of-gaussians approach. Additional tissue probability maps are also included as a priori information. In our case, we used as input the 15 $MPRAGE_{norm}$ images. The default options of the method were selected, including the use of the a priori tissue probability maps provided with SPM8. As a result, 6 tissue map classes were generated per subject. Each tissue map represents the probability that a voxel belongs to GM, WM, CSF, soft tissue, bone, or air.

The bone tissue probability maps were then eroded, following morphologic operations, to reduce potential artifacts that could arise from misclassifying some CSF voxels as bone. The eroded bone voxels were therefore assigned to the CSF class. Briefly, this process started by generating a brain-only mask combining and thresholding the GM, WM, and CSF tissue probability maps with a low threshold (0.2) to ensure that the brain mask did

not miss any potential voxels that were in fact brain voxels. This mask followed a morphologic closure with a structuring element of ones of size $7 \times 7 \times 7$ voxels to avoid potential gaps in the mask. Finally, the mask was eroded with a structuring element of ones of size $3 \times 3 \times 3$ voxels to ensure the brain-only mask was not larger to compromise true bone voxels to be properly classified. Sizes of the structuring elements for the morphologic operations (closure and erosion) were chosen following empiric evaluation of several subjects from the atlas-generation dataset. The voxels inside this final brain-only mask were zeroed in the bone probability map. Since the sum of all probability maps for all 6 tissue classes must remain constant (normalized to 1), these voxels were assigned to the CSF class.

Nonrigid Coregistration (SPM8 DARTEL Create Template). The tissue probability segments, obtained with the New Segment approach, were subsequently passed as inputs to the SPM8 DARTEL Create Template option. Details about the DARTEL (Diffeomorphic Anatomical Registration Through Exponentiated Lie Algebra) method were previously published (*2*). Briefly, DARTEL uses a constant velocity framework that allows quick estimation and invertible deformations to provide accurate nonrigid coregistration of images in an iterative fashion. In particular, SPM8 DARTEL is initialized with the tissue probability maps obtained from the New Segment step. At every iteration, the tissue probability maps are coregistered to a template given by the average of all subject classes obtained from the previous iteration. The accuracy and results of the DARTEL coregistration method were previously validated in comparison with 13 other nonrigid coregistration algorithms for brain imaging (*3*).

As a result, DARTEL produced a new tissue probability map template as well as accurate flow fields defining the large deformations (diffeomorphisms) needed to nonrigidly coregister the subject images to the new template. This template was used as the matching template for coregistering new subject images/tissue classes.

Nonrigid Warping (SPM8 Create Warped). The flow fields obtained with the DARTEL approach were used to nonrigidly deform (warp) the rCT images of all subjects included in the atlas formation dataset. This is achieved with the SPM8 Create Warped option. The new warped images, called CT_w, were therefore coregistered into the same space, defined here as atlas space.

Image Analysis

Tumor-to-brain ratios were calculated following a previously published method (*4*). Briefly, the slice with the highest tumor uptake on the PET_{CT} image was selected for all FET subjects. A circular ROI (25×25 mm) was drawn on the contralateral side on the same slice to serve as reference. The tumor ROI was defined using a minimum threshold of the mean plus 3 SDs of the reference ROI (*4*) on the PET_{CT} image. ROIs were then translated into the PET_{atlas} and PET_{Dixon} images. SUVmean and SUVmax from the tumor ROI were calculated, as well as the SUVmean for the reference ROIs. Mean and maximum T2B were computed by dividing, respectively, the SUVmean or SUVmax of the tumor ROI over the SUVmean of the reference ROI.

REFERENCES

1. Ashburner J, Friston KJ. Unified segmentation. *Neuroimage.* 2005;26:839–851.

2. Ashburner J. A fast diffeomorphic image registration algorithm. *Neuroimage.* 2007;38:95–113.

3. Klein A, Andersson J, Ardekani BA, et al. Evaluation of 14 nonlinear deformation algorithms applied to human brain MRI registration. *Neuroimage.* 2009;46:786–802.

4. Pauleit D, Stoffels G, Bachofner A, et al. Comparison of ^{18}F-FET and ^{18}F-FDG PET in brain tumors. *Nucl Med Biol.* 2009;36:779–787.

SUPPLEMENTAL TABLE 1. Summary of the 28 AAL Frontal Subregions

	ROIs	aRC (%)		naRC (%)	
		PET_{atlas}*	PET_{Dixon}*	PET_{atlas}*	PET_{Dixon}*
Validation dataset	1	6.24 ± 4.8	17.44 ± 8.46	–1.21 ± 5.12	–17.44 ± 8.46
	2	6.04 ± 4.56	17.04 ± 8.61	–1.18 ± 4.86	–17.04 ± 8.61
	3	6.29 ± 4.95	17.65 ± 7.81	–1.81 ± 5.31	–17.63 ± 7.83
	4	5.39 ± 4.09	15.7 ± 7.04	–1.72 ± 4.38	–15.69 ± 7.06
	5	3.14 ± 2.98	10.01 ± 4.02	–0.04 ± 3.26	–9.72 ± 4.24
	6	3.13 ± 2.62	9.59 ± 3.67	–0.61 ± 2.97	–9.35 ± 3.97
	7	6.28 ± 4.74	19.85 ± 9.68	–2 ± 5.07	–19.85 ± 9.68
	8	6.06 ± 4.64	17.97 ± 8.41	–1.37 ± 4.84	–17.97 ± 8.41
	9	3.98 ± 4.64	15.13 ± 7.9	0.24 ± 5.05	–14.93 ± 8.11
	10	3.81 ± 3.5	14.54 ± 7.47	–0.36 ± 3.95	–14.42 ± 7.6
	11	4.1 ± 3.68	15.9 ± 8.44	–1.17 ± 3.9	–15.9 ± 8.44
	12	3.96 ± 3	13.73 ± 6.87	–1.4 ± 3.35	–13.73 ± 6.87
	13	4.18 ± 3.41	17.45 ± 8.94	–1.14 ± 3.7	–17.45 ± 8.94
	14	4.71 ± 3.84	17.67 ± 10.02	–1.88 ± 4	–17.67 ± 10.02
	15	2.56 ± 2.07	11.35 ± 5.14	–0.52 ± 2.39	–11.35 ± 5.14
	16	3.53 ± 2.95	12.55 ± 7.05	–1.55 ± 3.19	–12.55 ± 7.05
	17	2.67 ± 2.25	11.99 ± 6.87	–1 ± 2.48	–11.99 ± 6.87
	18	3.48 ± 3.07	12.44 ± 7.96	–1.39 ± 3.32	–12.44 ± 7.96
	19	4.54 ± 2.11	12.38 ± 5.23	–2.08 ± 2.29	–12.38 ± 5.23
	20	4.37 ± 1.95	11.51 ± 4.47	–2.24 ± 2.17	–11.51 ± 4.47
	21	1.49 ± 0.52	4.86 ± 0.95	–0.78 ± 0.56	–4.86 ± 0.95
	22	1.66 ± 0.55	4.96 ± 0.92	–0.79 ± 0.6	–4.96 ± 0.92
	23	4 ± 3.03	14.27 ± 6.09	–1.15 ± 3.31	–14.27 ± 6.09
	24	4.04 ± 3.02	14.3 ± 5.42	–1.07 ± 3.32	–14.3 ± 5.42
	25	3.56 ± 4.28	10.77 ± 5.26	0.48 ± 4.43	–10.48 ± 5.45
	26	2.57 ± 2.39	9.32 ± 3.45	0.01 ± 2.56	–9.22 ± 3.56
	27	2.58 ± 2.15	6.73 ± 2.95	–1.08 ± 2.29	–6.56 ± 3.12
	28	2.34 ± 1.23	6.46 ± 1.87	–0.96 ± 1.36	–6.43 ± 1.92

*Average across subjects of the mean absolute and nonabsolute relative changes (aRC[%] and naRC[%], respectively) and SD.

1 = left precentral gyrus; 2 = right precentral gyrus; 3 = left superior frontal gyrus, dorsolateral; 4 = right superior frontal gyrus, dorsolateral; 5 = left superior frontal gyrus, orbital part; 6 = right superior frontal gyrus, orbital part; 7 = left middle frontal gyrus, lateral part; 8 = right middle frontal gyrus, lateral part; 9 = left middle frontal gyrus, orbital part; 10 = right middle frontal gyrus, orbital part; 11 = left opercular part of inferior frontal gyrus; 12 = right opercular part of inferior frontal gyrus; 13 = left area triangularis; 14 = right area triangularis; 15 = left orbital part of inferior frontal gyrus; 16 = right orbital part of inferior frontal gyrus; 17 = left rolandic operculum; 18 = right rolandic operculum; 19 = left supplementary motor area; 20 = right supplementary motor area; 21 = left olfactory cortex; 22 = right olfactory cortex; 23 = left superior frontal gyrus, medial part; 24 = right superior frontal gyrus, medial part; 25 = left superior frontal gyrus, medial orbital part; 26 = right superior frontal gyrus, medial orbital part; 27 = left gyrus rectus; 28 = right gyrus rectus.

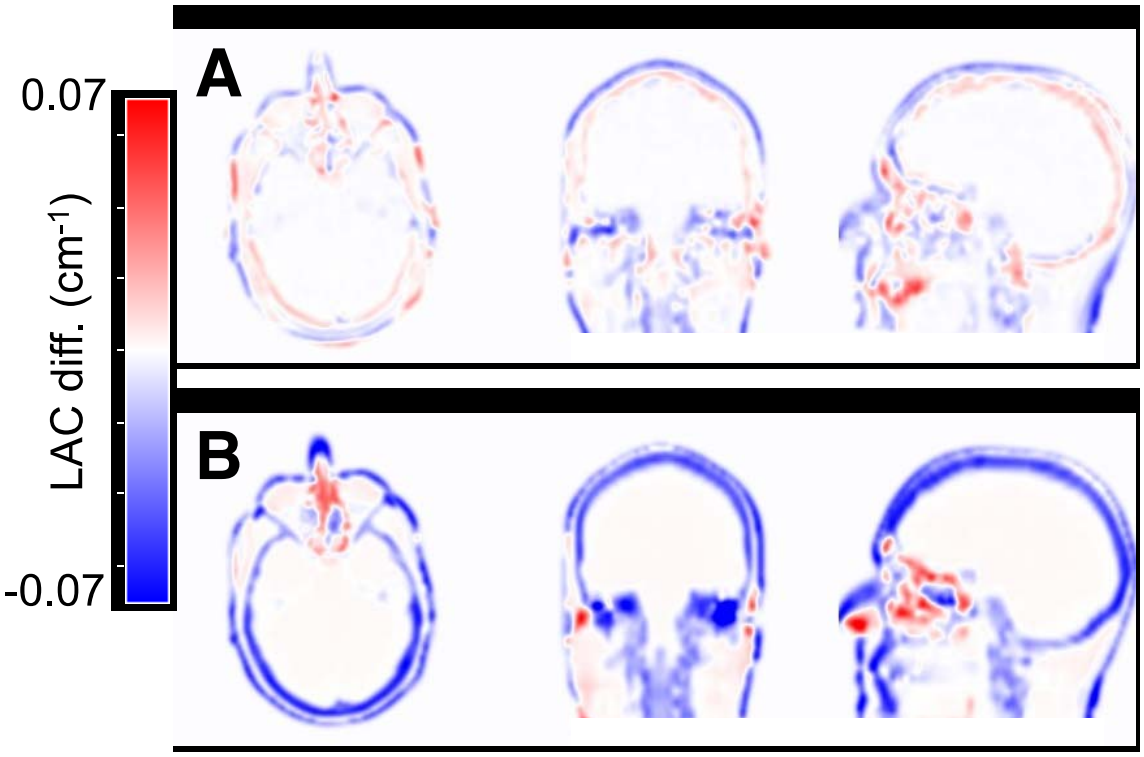

SUPPLEMENTAL FIGURE 1. Example of the differences between the LACs for one validation subject (from Fig. 2 in the article): differences between μ_{atlas} and μ_{CT} (A) and differences between μ_{Dixon} and μ_{CT} (B).

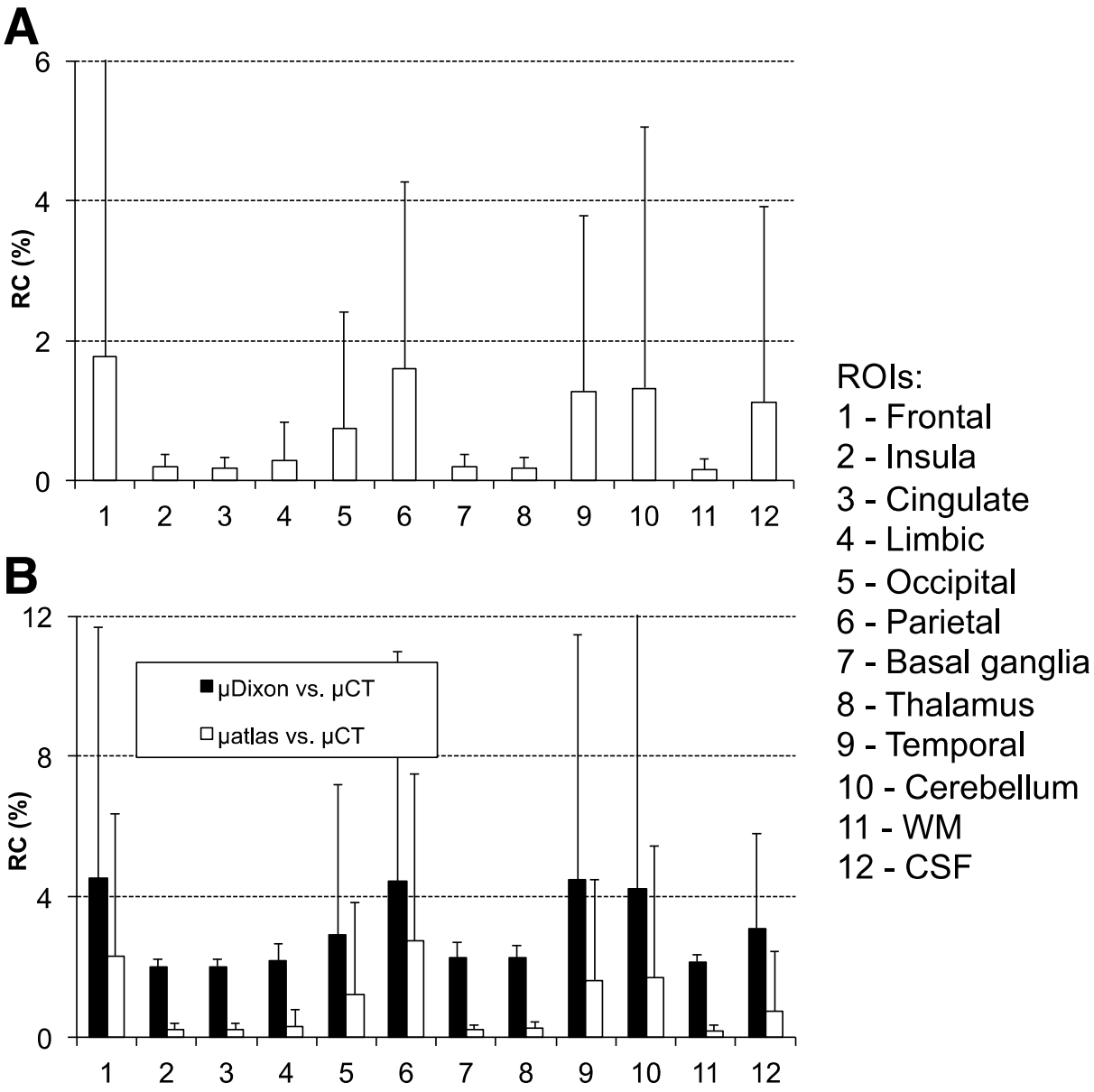

SUPPLEMENTAL FIGURE 2. ROI-based attenuation map comparison: $aRC\mu_{atlas}$ for all the atlas generation subjects (A) and $aRC\mu_{atlas}$ and $aRC\mu_{Dixon}$ for the validation subjects (B). Results are displayed as mean (and SD) of the absolute relative change (aRC) in %.

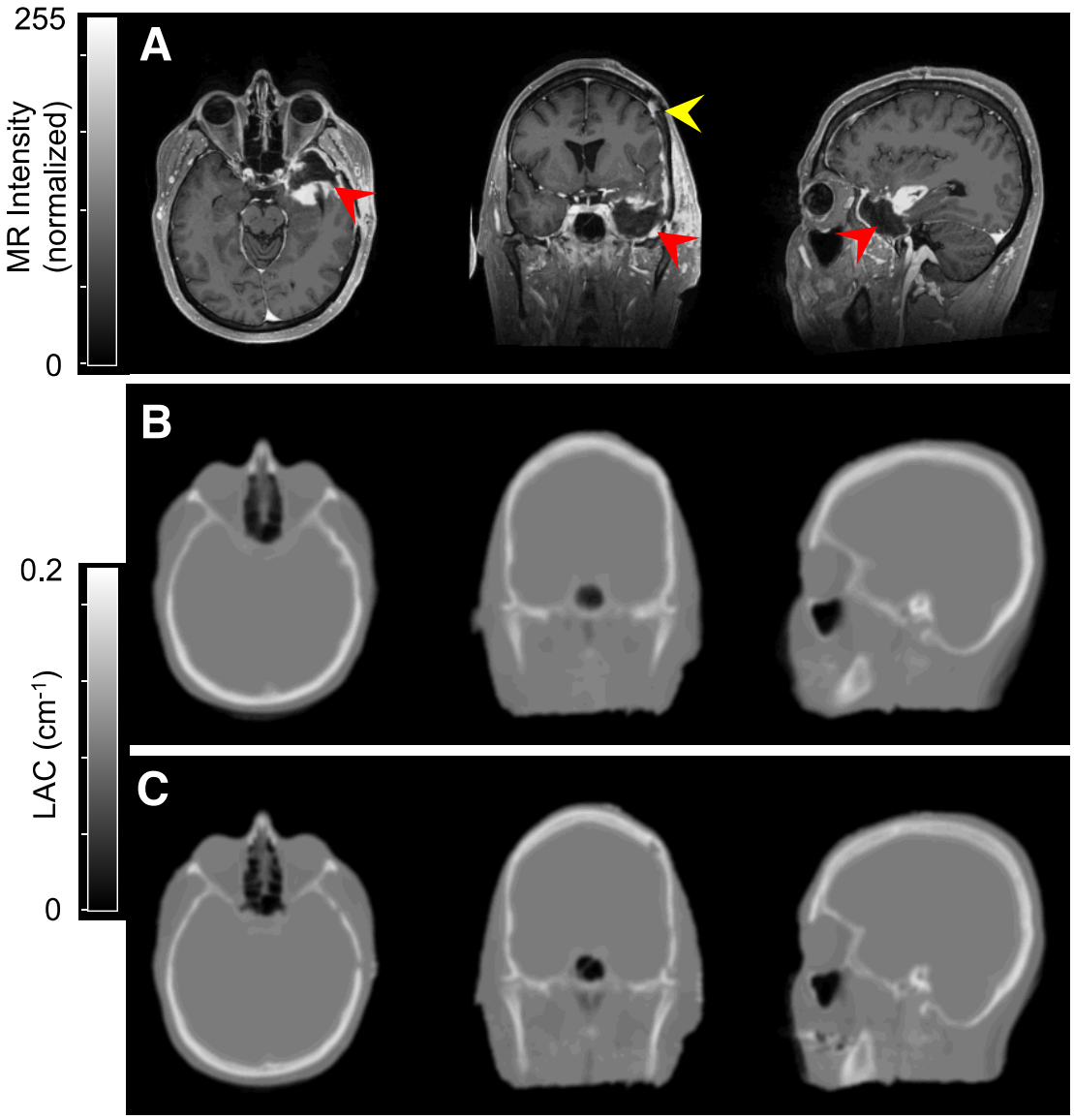

SUPPLEMENTAL FIGURE 3. Example of one challenging case from the atlas generation dataset showing a large tumor close to the bone (red arrowheads) as well as bone surgical alterations (yellow arrowhead): MR (A), μ_{atlas} (B), and μ_{CT} (C) images.

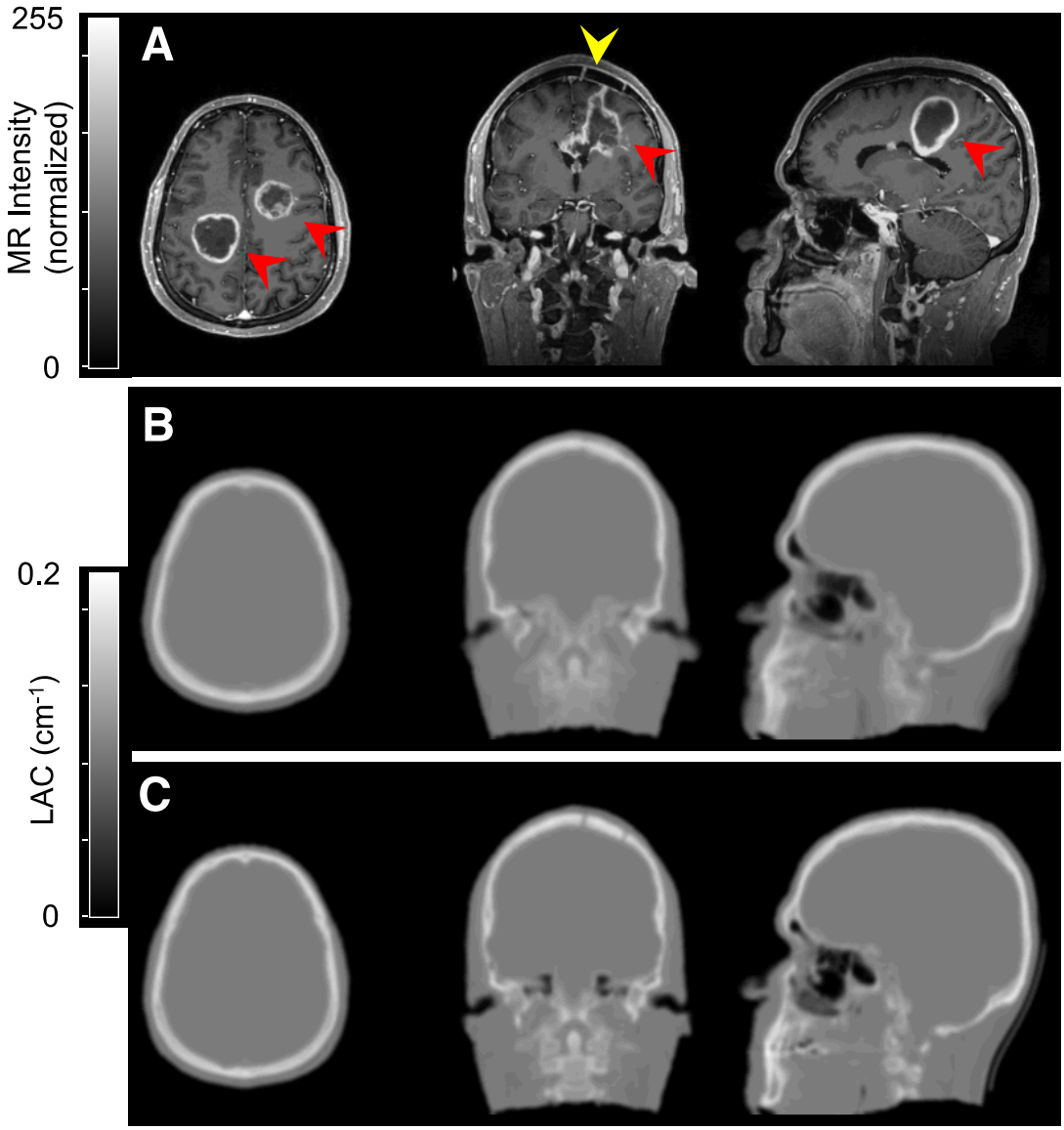

SUPPLEMENTAL FIGURE 4. Example of a challenging case from the atlas generation dataset showing 2 large lesions in both hemispheres (red arrowheads), as well as bone surgical alterations (yellow arrowhead): MR (A), μ_{atlas} (B), and μ_{CT} (C) images.

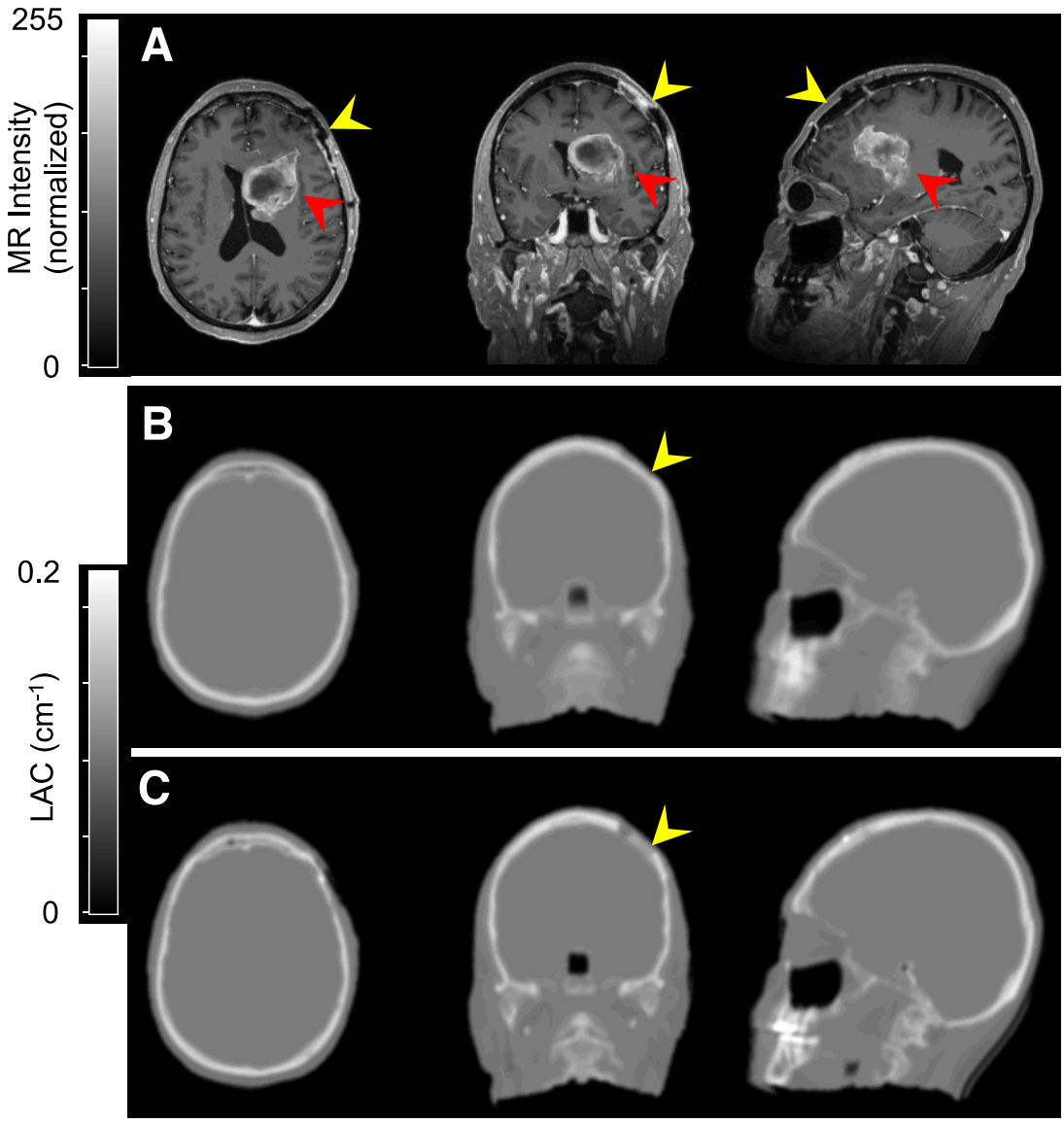

SUPPLEMENTAL FIGURE 5. Example of a challenging case from the atlas generation dataset showing 1 large tumor area in the ventricles (red arrowheads): MR (A), μ_{atlas} (B), and μ_{CT} (C) images. Note the thinner bone (yellow arrowhead) in the μ_{atlas} (and in μ_{CT}) after the surgical procedure.

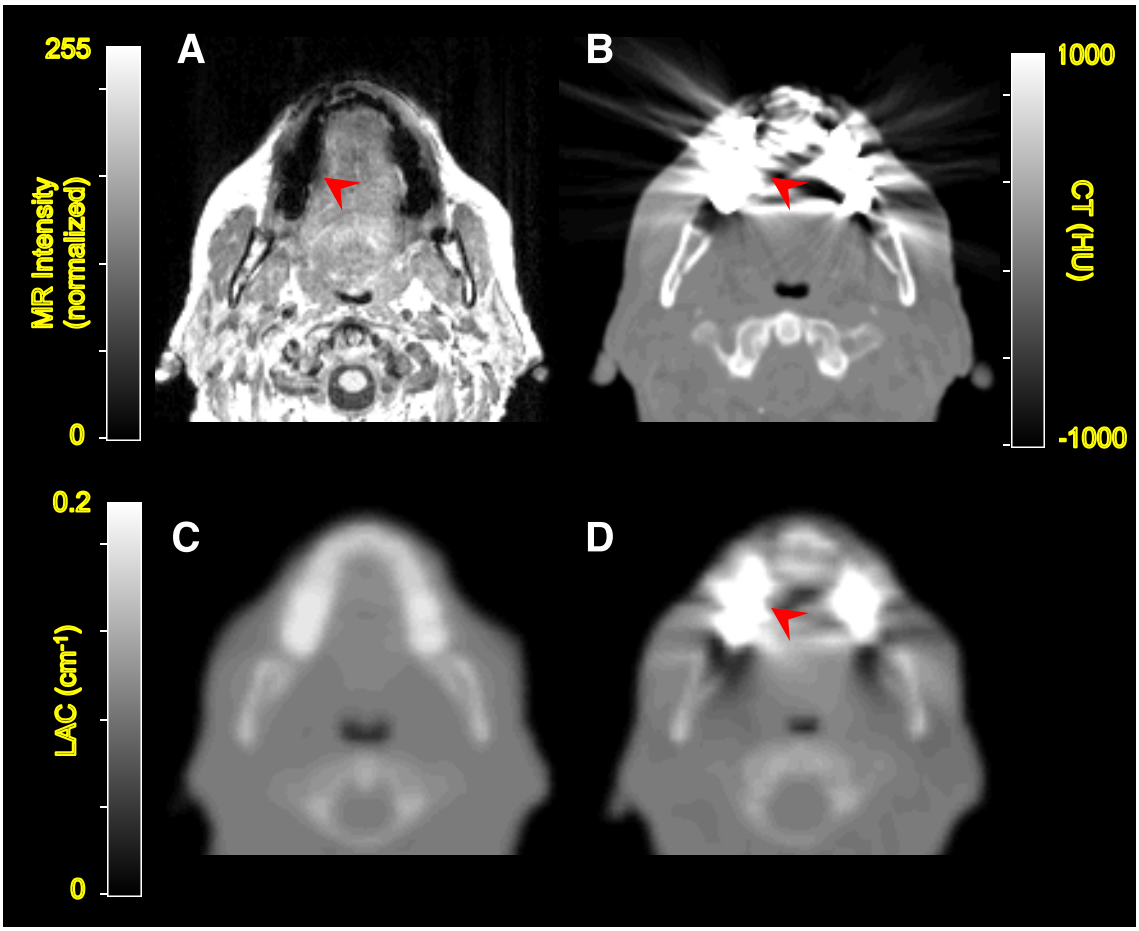

SUPPLEMENTAL FIGURE 6. Comparison of MR atlas– and CT-based attenuation map for a patient with dental work. Ovoid signal voids and streaking artifacts can be observed around the teeth (red arrowhead) in the MR image (A) and the corresponding CT image (B), respectively. No obvious artifacts are present in the μ_{atlas} (C) obtained from the MR data, whereas an overestimation of the LACs in the soft tissue surrounding the teeth can be observed in the μ_{CT} (D).